Hindawi
International Journal of Optics
Volume 2023, Article ID 3356849, 9 pages
https://doi.org/10.1155/2023/3356849

Research Article

The Optimization of Multimode Fiber Speckle Sensor for Microvibration

Haoyang Song, Feiyu Sun, Yunxu Sun , and Wei Liu

School of Electronics and Information Engineering, Harbin Institute of Technology, Shenzhen 518055, China

Correspondence should be addressed to Yunxu Sun; sunyunxu@hit.edu.cn

Received 25 October 2022; Revised 18 January 2023; Accepted 25 January 2023; Published 17 February 2023

Academic Editor: Sulaiman W. Harun

A vibration sensing system with optical fiber speckles is demonstrated and optimized with different optical fiber diameters and speckle statistical algorithms. The types of fiber diameter and material lead to a different performance of fiber specklegram sensor (FSS), which has been experimentally explored. The signal intensity, demodulated from the speckles, is different when using multimode fibers with different diameters. At the same time, the sensing effect of different fibers depends on the speckle statistical algorithms. Accordingly, we use different statistical methods in theory and experiment to analyze the influence of fiber diameter and speckle statistical methods on the sensing performance. A vibration sensing system with optimized performance is achieved by the optimized types of optical fiber and the corresponding optimized algorithms, which are promising for sensing weak vibration, such as detecting.

1. Introduction

Fiber specklegram sensors (FSS) are a kind of sensor based on the intermodal interference of multimode optical fibers (MMFs) [1]. When coherent light is incident into a multimode fiber, speckles will appear at the end of the multimode fiber. The FSSs are capable of performing similarly to the interferometric techniques [2], which have been used for measuring various physical parameters, such as measuring liquid refractive index [3], weight [4], temperature [5], lateral displacement [6], strain [7], vibration [8],and so on. Compared with interferometric optical fiber sensors, FSSs have the advantage of low cost, compared with other interferometric optical fiber sensors [9].

There are various schemes to retrieve sensing information from the specklegrams. The statistical methods calculate the correlations of specklegrams with outside disturbance, which include normalized inner-product [4], gray-levelco-occurrence matrix [7], first moment and second moment [9], the sum of squared differences [8], ratio image uniformity [10], mutual information [11], and so on. Machine learning is also used to recover information [12], but the calculation cost and sensing time are not satisfactory.

Silica MMFs and polymer optical fibers (POF) are two categories of MMFs. Silica MMFs with diameters of 50 or 62.5 microns are widely used in used for shorter-distance data transmission. POFs are made of polymer materials, typically polymethyl methacrylate (PMMA) polymer, which have been widely applied in data transmission and sensing [13]. Different types of MMFs lead to different types of specklegrams, which cause different statistical properties. Accordingly, the same speckle statistics method may lead to different statistics results for different types of MMFs, which may lead to different performances. It is important to choose a matching statistic method for the types of MMFs, which may optimize the measurement cost and sensing effect.

In this paper, the influence of optical fiber and speckle statistical algorithms with different parameters on vibration sensing is studied. By filtering the diameter of the optical fiber, we obtained the schemes to match the algorithm to MMFs for sensing vibration.

2. Materials and Methods

2.1. Fundamentals. There are many guiding modes of light in MMFs, and speckles are generated by interference between different modes at the end of fibers. When the fiber type, diameter, material, and wavelength of incident light are determined, the maximum number of modes in the fiber is also determined. Referring to Reference [13], the number of modes in step-index fiber, M, is given by the following equation:

$$M = \frac{V^2}{2}, \quad (1)$$

where V represents the normalized frequency in the fiber, which can be expressed by the following equation:

$$V = \frac{2a\pi\sqrt{\left(n_1^2 - n_2^2\right)}}{\lambda}, \quad (2)$$

where a is the core radius of fiber, λ is the wavelength of light, n_1 is the core index of refractive, and n_2 is the cladding index of refractive. Different diameters of optical fibers have different numbers of modes, which will lead to the number of speckle granules in the specklegram output at the end of the fiber, and further affect the sensing sensitivity [13].

It is assumed that the illuminating light emitted into the optical fiber is emitted from a highly coherent light source, and all modes in the optical fiber are excited. Referring to [1], the far-field complex speckle distribution of the fiber is a coherent superposition of the complex amplitudes of all modes, such as

$$A(x, y) = \sum_{m=0}^{M} a_m(x, y)\exp\left[j\phi_m(x, y)\right]. \quad (3)$$

The light intensity measured by CCD can be expressed by the following equation:

$$I(x, y) = \sum_{m=0}^{M}\sum_{n=0}^{M} a_m a_n \exp\left[j\left(\phi_m - \phi_n\right)\right], \quad (4)$$

where a_m, ϕ_m are the m-th mode's amplitude and phase, and are the n-th mode's amplitude and phase.

The statistical information of the specklegram represents the sensing information. In this paper, the normalized innerproduct coefficient, gray-levelco-occurrence matrix, first moment, and zero mean normalized cross-correlation are utilized to demodulate the vibration information, which is depicted as follows.

2.1.1. Normalized Innerproduct Coefficient (NIPC). The specklegrams are containing position information and light intensity information. NIPC is used as the statistical characteristic value of the specklegrams for theoretical analysis, and the relationship between the statistical characteristic value of the speckle and the external disturbance is established. NIPC value is given by the following equation:

$$\mathrm{NIPC}(k) = \frac{\int\int I_0 I \,\mathrm{d}x\mathrm{d}y}{\left(\int\int I_0^2 \mathrm{d}x\mathrm{d}y \int\int I^2 \mathrm{d}x\mathrm{d}y\right)^{1/2}}, \quad (5)$$

where I_0 indicates the light intensity at position (x, y) in the reference specklegram, and I indicates the light intensity at position (x, y) in the measuring specklegram.

2.1.2. Gray-LevelCo-Occurrence Matrix (GLCM). GLCM is a square matrix related to the texture of the image. The elements of the matrix are equal to the number of gray levels in the image. The GLCM is calculated to show how often a pixel with gray-level (or grayscale intensity) value i occurs to adjacent pixels with the value j. If the size of the image is $M \times N$, the gray level is G, and its $G \times G$ size GLCM matrix. The elements can be expressed as

$$M_G(i, j) = \sum_{x=1}^{M}\sum_{y=1}^{N}\begin{cases} 1, & \text{if } P(x, y) = i \,\&\, P\left(x + d_x, y + d_y\right) = j, \\ 0, & \text{otherwise,} \end{cases} \qquad 1 \le i,\ j \le G. \quad (6)$$

Among them, $P(x, y)$ represents the selected pixel and $d(d_x, d_y)$ represents the offset value.

The eigenvalues of the gray-levelco-occurrence matrix are contrast, autocorrelation, entropy, and homogeneity. In sensing, the eigenvalues of the contrast and homogeneity of the gray-levelco-occurrence matrix are used as the statistical eigenvalues of speckles. Homogeneity, which measures the closeness of the distribution of elements in the GLCM to the GLCM diagonal, is given by the following:

$$\mathrm{HOM} = \sum_{i}^{G}\sum_{j}^{G} M_G \frac{(i, j)}{(1 + |i - j|)}. \quad (7)$$

The contrast, which represents the clarity of the image and the depth of the texture groove, is given by the following equation:

$$\mathrm{CON} = \sum_{i}^{G}\sum_{j}^{G} (i - j)^2 M_G(i, j). \quad (8)$$

2.1.3. First Moment/Second Moment. The first moment refers to associating the position information with the intensity on each pixel in the category of the matrix, which is an analogoue of the moment of a flat plate with uneven mass distribution in mechanics. The mean values in the x and y directions, μ_x and μ_y are given as follows:

$$\mu_x = \frac{\sum_{x,y} x I(x,y)}{\sum_{x,y} I(x,y)},$$
$$\mu_y = \frac{\sum_{x,y} y I(x,y)}{\sum_{x,y} I(x,y)}. \quad (9)$$

The general formula of the p-th radial moment is given by the following equation:

$$\mu_p = \frac{\sum_{x,y}\left[(x-\mu_x)^2 + (y-\mu_y)^2\right]^{p/2} I(x,y)}{\sum_{x,y} I(x,y)}. \quad (10)$$

Although the expressions of the first moment and the second moment are different in value, the overall trend is the same. Therefore, it can be regarded as achieving similar statistical effects with the first moment and the second moment.

2.1.4. Zero Mean Normalized Cross-Correlation (ZNCC). In ZNCC, the intensity of each pixel in the specklegram is subtracted from its own mean value, to calculate the correlation. Accordingly, ZNCC is more robust to linear and uniform brightness changes, which is given by the following equation:

$$\mathrm{ZNCC}(k) = \frac{\sum^N (I_0 - \bar{I}_0)(I - \bar{I})}{\left[\sum^N (I_0 - \bar{I}_0)^2 (I - \bar{I})^2\right]^{1/2}}. \quad (11)$$

Similar to the NIPC algorithm, when the reference specklegram is the same as the measured specklegram, the value is 1. When the specklegram deviates from the reference specklegram, ZNCC will decrease accordingly. I_0 can be set as a calibration point, which can improve the dynamic range of the measurement. It is different from the NIPC algorithm.

2.2. Experiment Setup. The experimental setup for the speckle vibration sensing system is shown in Figure 1. The light source is a semiconductor laser of 650 nm. A CCD (Hikvision MV-CA013-21UM, USB3.0) acquires the specklegram from the MMFs, which is set at 30FPS. According to the Nyquist sampling law, we can measure vibration signals below 15 Hz.

In this paper, we choose 4 types of step-type silica MMFs and 3 types of POFs made of PMMA with different diameters and numerical aperture (NA), provided commercially, which are shown in Table 1.

Vibration on fiber is excited by the motor, which is set at the speed of 26.5 rpm (round per minute, RPM). The corresponding frequency of vibration is 0.4417 Hz. The vibration can be represented by the change of speckle statistics of the fiber specklegram. Here we choose seven commercial optical fibers, as shown in Table 1. Under the disturbance of the vibration signal of fixed frequency, the specklegrams were acquired continuously for two minutes with CCD at the acquisition speed of 30 frames per second (FPS), which forms an independent data set. The corresponding sensing curve can be obtained by processing the specklegrams with different speckle statistical methods, and the sensing curve takes time as the horizontal axis. Repeating the experiment 5 times to take the average value.

As the core diameter of the same fiber increases, the size of the speckle granules gradually decreases, and the number of speckle granules gradually increases, as shown in Figure 2. Based on the known fiber parameters and the wavelength information of the light source, we can calculate the maximum number of modes that can be transmitted in different fibers. The maximum number of modes M that can be transmitted by stepped silica fibers has been given in Table 1. Theoretically, a larger diameter of the fiber supports more number of modes transmitted in the fiber, which affects the sensitivity of FSSs.

3. Results and Discussion

3.1. Sensing Results of Vibration. Ideally, when the fiber is not disturbed, the speckle statistics value should remain constant. However, due to temperature drift and other NOSIE, the statistical value is not constant. Here, we test the stability of sensing systems by getting specklegrams without vibration. The standard deviation of the sensing value describes the stability of the sensing process. Under the same set of data, the coefficients of variation are 1.5837×10^{-6} (NIPC), 5.3349×10^{-3} (GLCM-contrast), 1.7229×10^{-3} (GLCM-homogeneity), 0.9414×10^{-4} (first-moment), and 1.6269×10^{-5} (ZNCC). NIPC and ZNCC have good stability.

Figure 3 shows the speckle vibration frequency sensing curve of the silica step-index fiber with different core diameters and polymer fibers based on the NIPC method and its fast Fourier transform image. The baseline is fitted by the least square and is removed.

In Figure 3, the vibration signals based on fibers with different diameters are demodulated by NIPC. The peaks of the curve reflect the sensitivity of sensing. With the same vibration, the curves of NIPC values of different fibers are different. As the fiber core diameter increases, the sensing value gradually increases. But when the diameter becomes larger to a certain value, the amplitude of the sensing curve shows a downward trend. When the linearity of the vibration sensing curve becomes very poor, the tiny vibration signal will vanish in the sensing system.

The main frequency of the vibration sensing curve after the Fourier transform can be used as the recovered vibration frequency. It can be seen that the specklegrams from various optical fibers have demodulated the vibration frequency information. Except for the slightly different recovery results of 50 μm silica fiber, the recovery results of other diameters are very accurate. In addition, it can also be combined with the linearity of the NIPC vibration sensing curve to evaluate the sensing quality. For example, in Figure 3(g), for a vibration signal with a fixed amplitude, the response to the vibration signal becomes smaller and smaller with time, and the distortion of the sensing curve is serious.

GLCM vibration sensing curves of fibers with core diameters of 105 μm and 250 μm are shown in Figure 4. After the fast Fourier transform, only silica fibers with core diameters of 105 μm and 200 μm and polymer fibers with

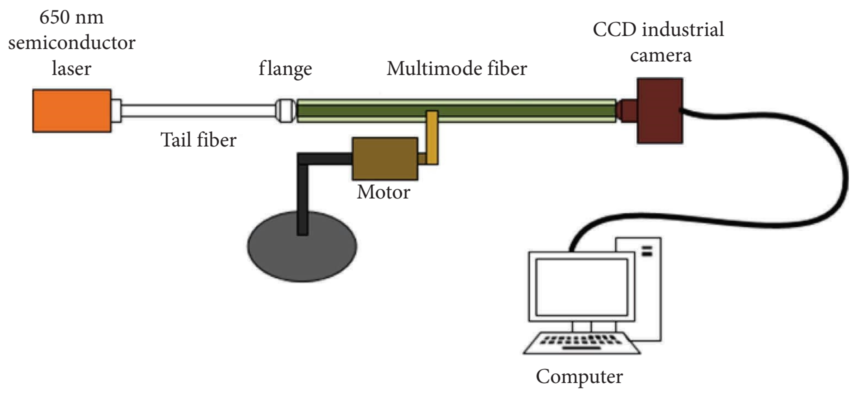

Figure 1: Structure of fiber specklegram sensor. The vibration sensor structure built in this paper is composed of a 650 nm semiconductor laser light source, multimode fiber, a CCD camera, and a DC deceleration motor.

Table 1: Type of fibers selected in the experiment.

Material	Diameter (μm)	NA	Length (m)	Maximum number of modes
Silica	50	0.22	1	1.41×10^3
Silica	62.5	0.22	1	2.21×10^3
Silica	105	0.22	1	6.23×10^3
Silica	200	0.22	1	2.26×10^3
PMMA	250	0.5	0.6	1.82×10^5
PMMA	500	0.5	0.6	7.3×10^5
PMMA	1000	0.5	0.6	2.92×10^6

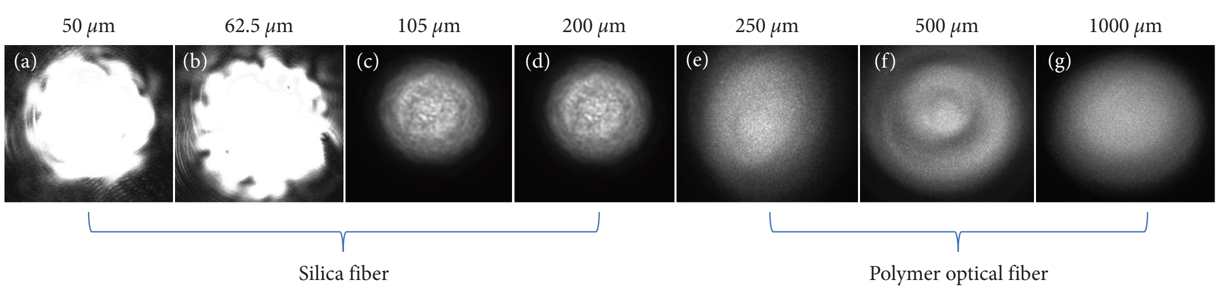

Figure 2: Optical fiber specklegrams formed by fibers with different core diameters: (a) 50 μm silica fiber, (b) 62.5 μm silica fiber, (c) 105 μm silica fiber, (d) 200 μm silica fiber, (e) 250 μm polymer optical fiber, (f) 500 μm polymer optical fiber, and (g) 1000 μm polymer optical fiber.

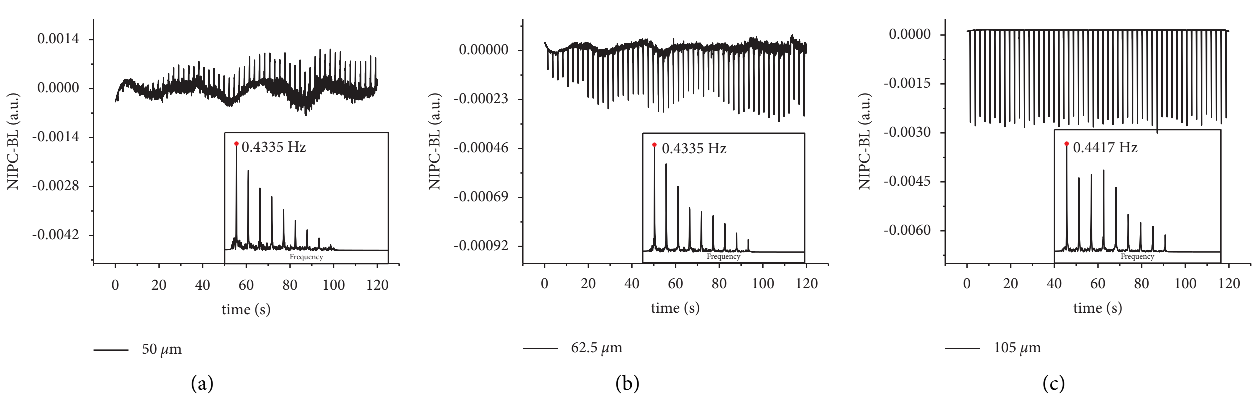

Figure 3: Continued.

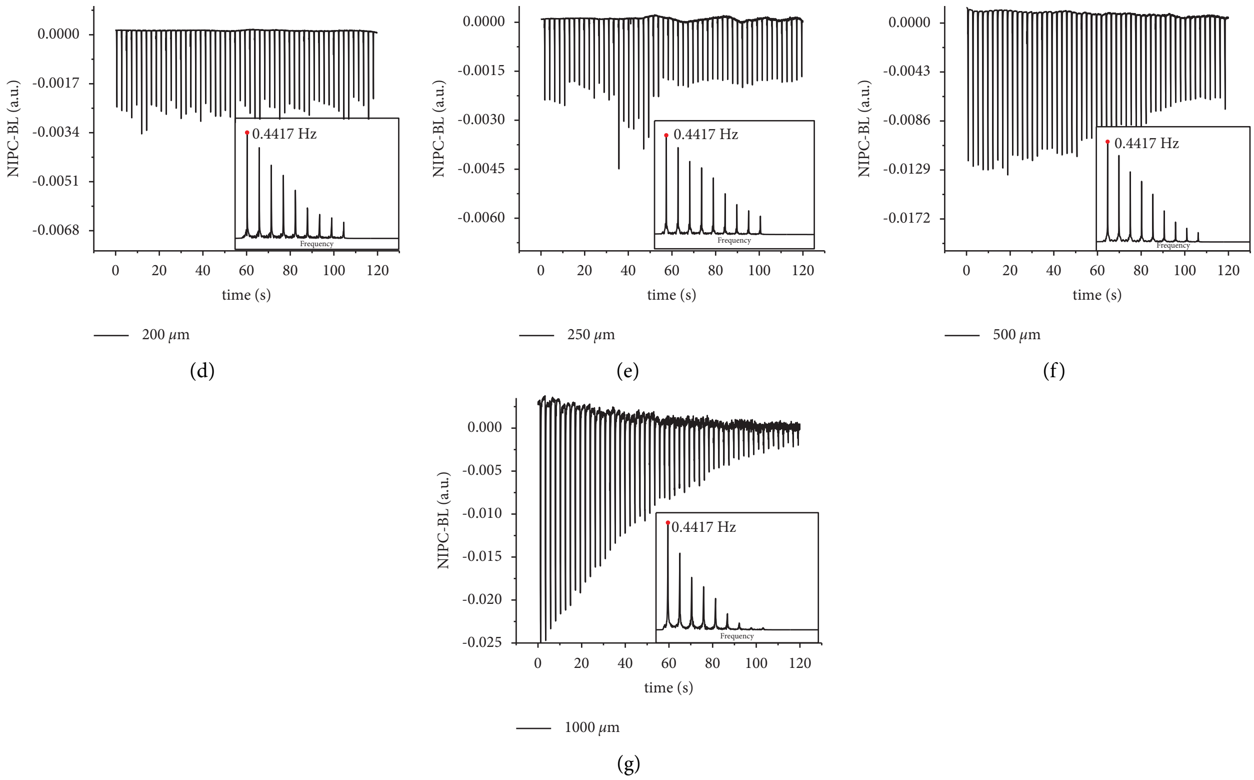

Figure 3: NIPC curve of vibration. NIPC curve of quartz step fiber: (a) 50 μm silica fiber; (b) 62.5 μm silica fiber; (c) 105 μm silica fiber; (d) 200 μm silica fiber; (e) 250 μm silica fiber; (f) 500 μm polymer optical fiber; (g) 1000 μm polymer optical fiber Inset: FFT curve.

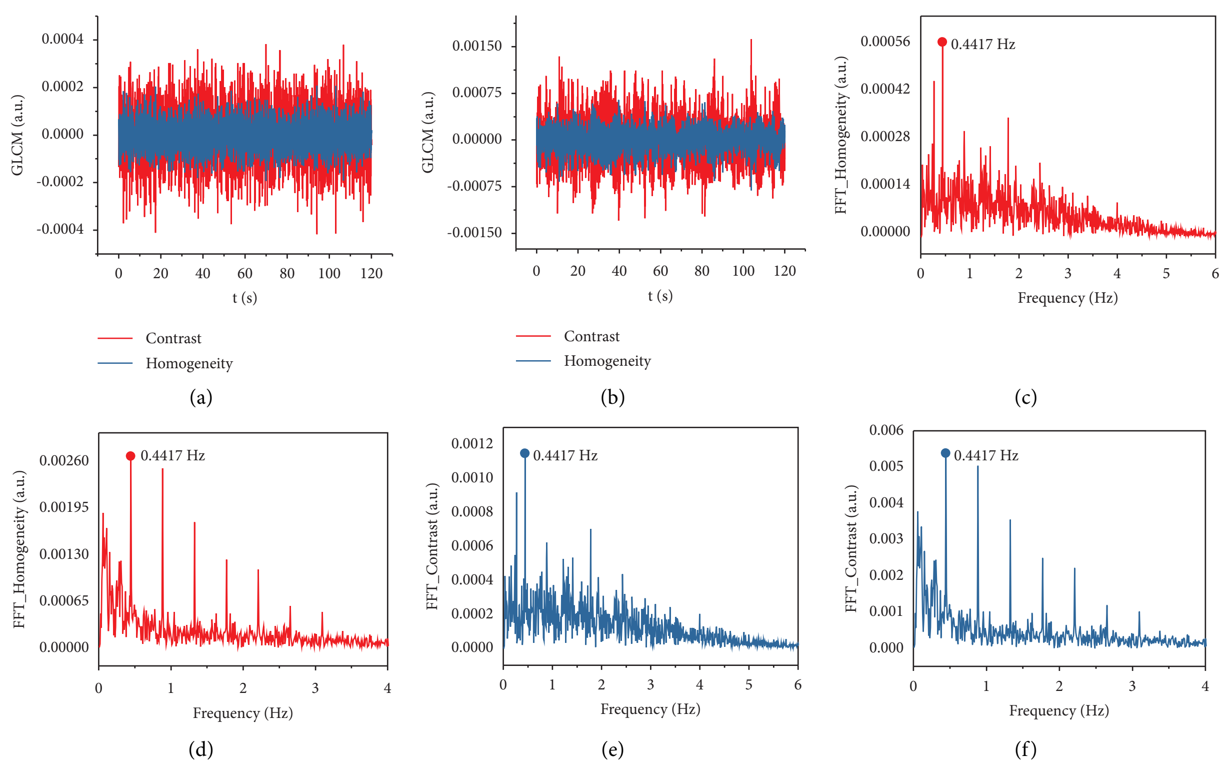

Figure 4: GLCM vibration sensing curves of fibers with different core diameters (red: contrast, blue: homogeneity): (a) 105 μm polymer optical fiber, (b) 250 μm polymer optical fiber, (c) FFT-contrast sensing curve of 105 μm polymer optical fiber, (d) FFT-contrast sensing curve of 250 μm polymer optical fiber, (e) FFT-homogeneity sensing curve of 105 μm polymer optical fiber, and (f) FFT-homogeneity sensing curve of 250 μm polymer optical fiber.

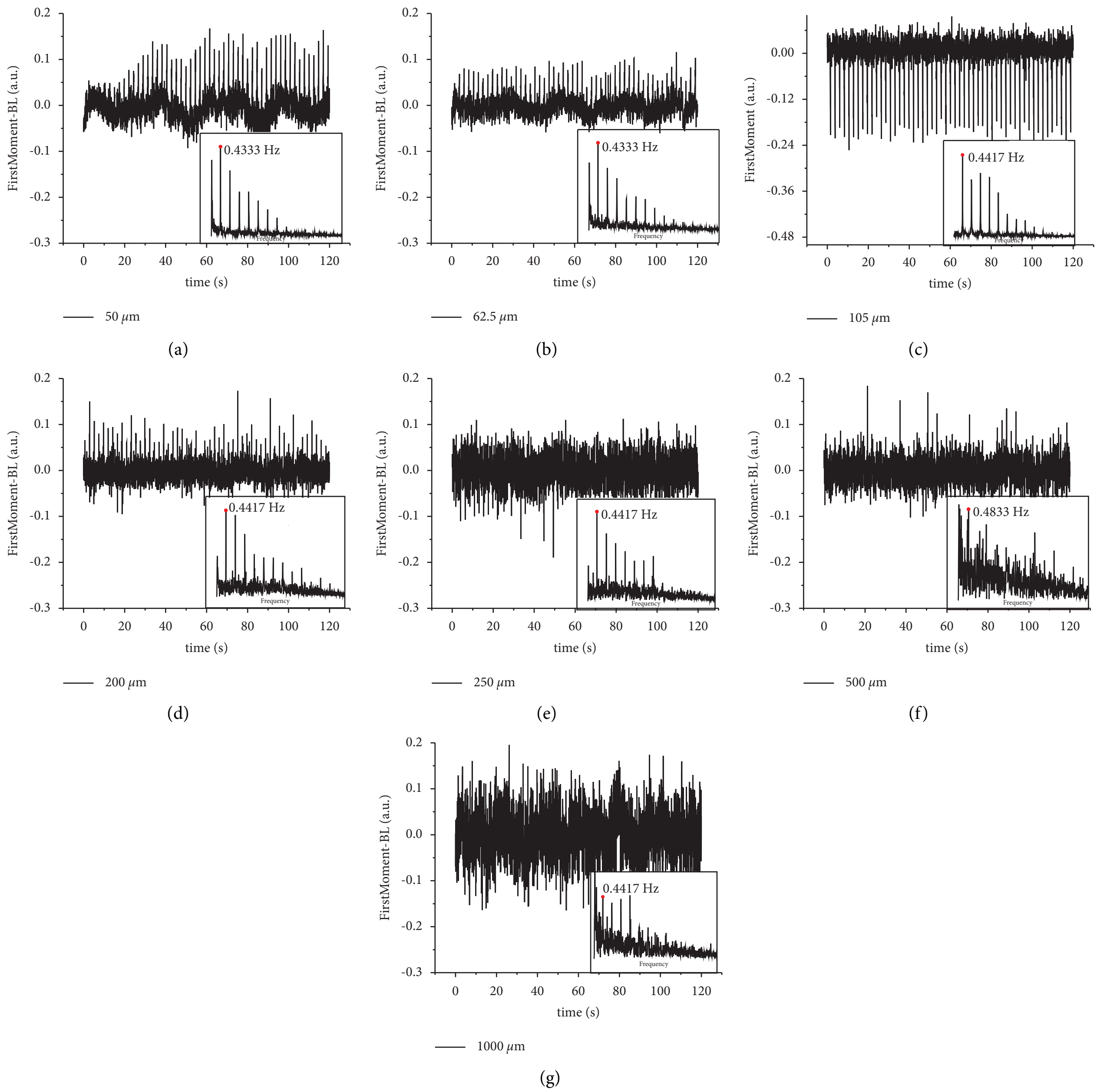

Figure 5: First-moment curve of vibration. The first-moment curve of different fibers: (a) 50 μm silica fiber, (b) 62.5 μm silica fiber, (c) 105 μm silica fiber, (d) 200 μm silica fiber, (e) 250 μm silica fiber, (f) 500 μm polymer optical fiber, and (g) 1000 μm polymer optical fiber. Inset: FFT curve.

250 μm can demodulate the vibration signal, while others fail. The sensing curve of the contrast characteristic value in GLCM and the main frequency amplitude are much greater than the homogeneity characteristic value in GLCM.

For the results of the first moment in Figure 5, for the silica fibers, the periodic pulse peaks are distinguished, and the main frequency after demodulation is also accurate, with 200 μm being the best. For the POFs, the pulse peak is not obvious, and the frequency cannot be calculated. Only 250 μm polymer optical fiber can demodulate the valid vibration signal frequency information. Some of the others can also demodulate information, but its amplitude is equivalent to or smaller than the amplitude of the interference frequency.

In Figure 6, the ZNCC sensing curves obtained by the sensing system, give obvious periodic pulse peaks. However, the sensing curve after preprocessing still fluctuates. As the fiber core diameter increases, the peak value of the pulse peak in the sensing curve shows an upward trend. However, as the fiber core diameter increases and exceeds a certain value, the linearity of the system sensing curve shows a downward trend.

3.2. Discussion. For the same specklegrams, the four speckle statistical methods exhibit different performances. Ideally, for the same vibration signal, the larger the diameter of the

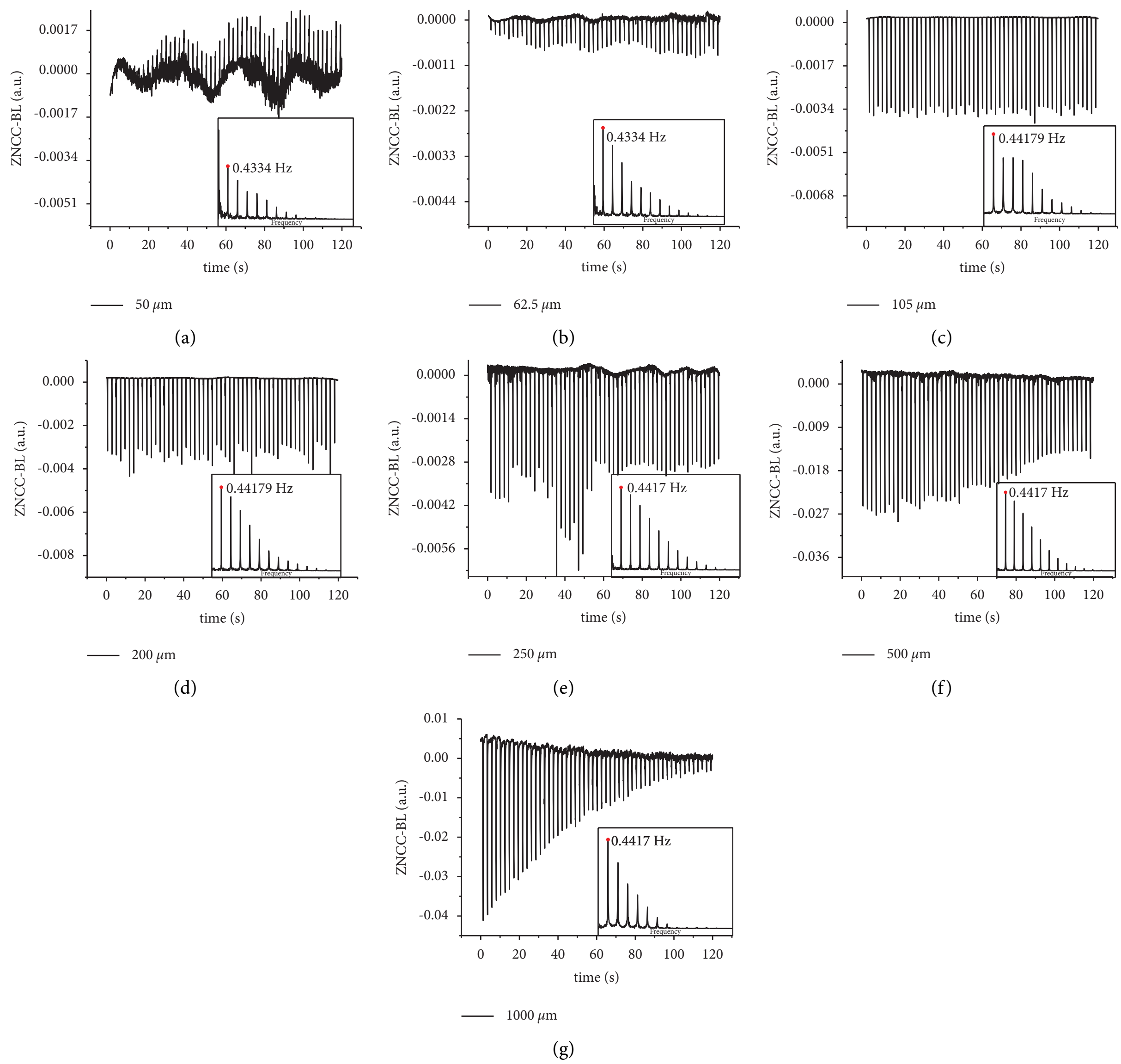

Figure 6: ZNCC curve of fibers vibration. ZNCC curve of different fibers: (a) 50 μm silica fiber, (b) 62.5 μm silica fiber, (c) 105 μm silica fiber, (d) 200 μm silica fiber, (e) 250 μm silica fiber, (f) 500 μm polymer optical fiber, (g) 1000 μm polymer optical fiber. Inset: FFT curve of fibers.

fiber is, the larger the peak amplitude of the sensing curve pulse is and the more accurate the FFT frequency is. However, due to the increase of modes, the influence of interference will grow greater in the experiment.

For all the speckle statistical methods, a thin optical fiber always has less speckle information. The statistical value fluctuates greatly, which leads to a nonhorizontal baseline, as shown in Figure 3(a). A large diameter eliminates this problem of baseline. Each speckle statistical method demodulates the vibration signal by calculating the changes in speckle images. When the number of speckles is too low, the statistical values cannot reflect the vibration signal well.

On the contrary, if the speckle granules are too small, the CCD may not be able to capture them. A high-resolution camera is needed, which increases the cost of the sensor. Furthermore, the influence of disturbance on speckles will also increase with the increase in the number of modes. The influence of interference on speckles will also increase with the increase in the number of modes. These influences gradually overlap. Finally, the pulse amplitude of the sensing curve becomes uneven with gradually decreasing, shown in Figure 3(k) and Figure 6(g).

In the experiments to test the stability of the algorithm, the sensing values of ZNCC and NIPC are basically constant. NIPC and ZNCC methods are cross-correlations between the intensity information and spatial information. For fibers of different diameters, the sensing curve has obvious repetitive pulse peaks, and the number of times matches the set frequency. ZNCC can also adjust the I_0 point by itself to improve the dynamic range, which improves the linear range and improve the sensitivity of the sensor by manually zeroing. In addition, a timely update of reference pictures can also reduce drift caused by environmental interference,

Table 2: Matching scheme of the vibration sensing system.

	Silica step-index fiber (μm)	POF (μm)
NIPC	200	500
GLCM	105	250
First moment	200	250
ZNCC	200	500

and avoid linearity degradation caused by excessive baseline floating.

In contrast, the GLCM algorithm still has strong fluctuations in sensing data even without vibration. When the experimental fiber becomes larger, the number of modes will increase, and the influence of disturbance will become larger, accordingly, the oscillation of the sensing curve will become more obvious. When performing low-frequency vibration sensing, the distinction between the vibration signal and the interference signal is low. At the experimental frequency, even if the data has been preprocessed, the sensing curve still cannot form an obvious periodic pulse peak. As shown in Figure 5, only two sensing curves can demodulate the external vibration signal.

The stability of FM is between GLCM and ZNCC, under appropriate diameters, which demodulate obvious periodic pulse peaks. However, there are many burrs in the pulse curve, and the main frequency of FFT is not clearly distinguished from other frequencies.

Optimized statistical methods should be selected for fibers of different diameters, based on criteria such as a smooth sensing curve, a uniform periodic pulse peak, and distinct main frequency amplitude after FFT. Based on the above selection criteria, the matching scheme of the vibration sensing system can be given, as shown in Table 2.

4. Conclusions

Several statistical methods are introduced, and the optimization analysis of vibration sensing is performed with the addition of low-frequency vibration signals. Both NIPC and ZNCC show good stability and can recover more accurate sensing information for fibers of different diameters. ZNCC can adjust the dynamic range by zeroing, making the application scenarios of vibration sensing wider. GLCM can very finely reflect the texture of the image and accurately reflect the weak change of the fiber state, but in the low-frequency vibration sensing scene, its demodulation and stability are not good. FM also has stability problems. The trend of the corresponding P-th moment algorithm is the same, but the amplitude is different. This feature can be used to adjust application scenarios.

When there is less speckle information for a 50 μm silica fiber, the sensing curve of each statistical method still fluctuates after baseline fitting, which affects the frequency recovery. The larger diameter of the fiber, the greater the peak amplitude of the sensing curve pulse, and the higher the demodulated main frequency amplitude. However, affected by stability, the more modes, the more affected the amplitude of the pulse peak, and the higher the requirements for sampling equipment.

Finally, for different speckle statistical methods, suggested fiber diameters for vibration sensing systems are given.

Data Availability

The data used in this study are generated from the measures in the paper.

Conflicts of Interest

The authors declare that they have no conflicts of interest regarding the publication of this paper.

Authors' Contributions

Haoyang Song and Feiyu Sun contributed equally to this work.

Acknowledgments

This study is funded by Science and Technology Planning Project of Shenzhen Municipality (JCYJ20190806142610885), China.

References

[1] F. T. S. Yu, J. Zhang, S. Yin, and P. B. Ruffin, "Analysis of a fiber specklegram sensor by using coupled-mode theory," *Applied Optics*, vol. 34, no. 16, pp. 3018–3023, 1995.

[2] E. Fujiwara, Y. T. Wu, and C. K. Suzuki, "Vibration-based specklegram fiber sensor for measurement of properties of liquids," *Optics and Lasers in Engineering*, vol. 50, no. 12, pp. 1726–1730, 2012.

[3] J. J. Wang, S. C. Yan, Y. P. Ruan, F. Xu, and Y. Q. Lu, "Fiber-Opticpoint-based sensor using specklegram measurement," *Sensors*, vol. 17, no. 10, p. 2429, 2017.

[4] F. T. S. Yu, M. Wen, S. Yin, C. M. Uang, and Uang, "Submicrometer displacement sensing using inner-product multimode fiber speckle fields," *Applied Optics*, vol. 32, no. 25, p. 4685, 1993.

[5] M. J. Murray, A. Davis, C. Kirkendall, and B. Redding, "Speckle-based strain sensing in multimode fiber," *Optics Express*, vol. 27, no. 20, Article ID 28494, 2019.

[6] W. B. Spillman, B. R. Kline, L. B. Maurice, and P. L. Fuhr, "Statistical-mode sensor for fiber optic vibration sensing uses," *Applied Optics*, vol. 28, no. 15, pp. 3166–3176, 1989.

[7] Y. Liu, Q. Qin, H.-h. Liu, Z.-w. Tan, and M.-g. Wang, "Investigation of an image processing method of step-index multimode fiber specklegram and its application on lateral displacement sensing," *Optical Fiber Technology*, vol. 46, pp. 48–53, 2018.

[8] L. M. Gevrekci, M. U. Demircin, and E. Akagunduz, "Real-time image registration," in *Proceedings of the 20th Signal Processing and Communications Applications Conference (SIU)*, Mugla, Turkey, April 2012.

[9] H. S. Efendioglu, T. Yildirim, O. Toker, and K. Fidanboylu, "New statistical features for the design of fiber optic statistical mode sensors," *Optical Fiber Technology*, vol. 19, no. 4, pp. 279–284, 2013.

[10] D. L. G. Hill, P. G. Batchelor, M. Holden, and D. J. Hawkes, "Medical image registration," *Physics in Medicine and Biology*, vol. 46, no. 3, pp. 1–45, 2001.

[11] Brunelli and Roberto, *Template Matching Techniques in Computer Vision || Building a Multibiometric System*, Wiley, New York, NY, USA, 2009.

[12] E. Fujiwara, Y. Ri, Y. T. Wu et al., “Evaluation of image matching techniques for optical fiber specklegram sensor analysis,” *Applied Optics*, vol. 57, no. 33, pp. 9845–9854, 2018.

[13] Z. Xiaomin, S. Yunxu, X. Fucheng, M. Yan, and Z. Jianyu, “Research on the measurement of heart rate based on LD laser and multimode fiber,” in *Proceedings of the 2020 IEEE 5th Optoelectronics Global Conference*, pp. 200–203, Shenzhen, China, September 2020.